

# A Computer Code for Performance of Spur Gears\*

K. L. Wang†, and H. S. Cheng‡

In spur gears both performance and failure predictions are known to be strongly dependent on the variation of load, lubricant film thickness, and total flash or contact temperature of the contacting point as it moves along the contact path. The need of an accurate tool for predicting these variables has prompted the development of a computer code (refs. 1 and 2) based on recent findings in EHL and on finite-element methods. This paper gives a brief summary of the analyses and some typical results to illustrate effects of gear geometry, velocity, load, lubricant viscosity, and surface convective heat transfer coefficient on the performance of spur gears.

## Symbols

Values are given in both SI and U.S. Customary Units. The calculations were made in U.S. Customary Units.

$C_o$	damping coefficient per unit face width, N·s/m <sup>2</sup> , (lb·s/in <sup>2</sup> )
$e_a, e_b$	profile error for meshing set $a, b$ , m (in.)
$h_{\min}$	minimum film thickness, m (in.)
$I_1, I_2$	polar mass moment of inertia of pinion and gear, kg·m <sup>2</sup> (slug·in <sup>2</sup> )
$K$	stiffness of a meshing pair, N/m <sup>2</sup> (lb/in <sup>2</sup> )
$K_a, K_b$	$K$ for meshing set $a, b$ , N/m <sup>2</sup> (lb/in <sup>2</sup> )
$M$	effective mass = $m_1 m_2 / (m_1 + m_2)$ , kg (slug)
$m_1, m_2$	mass of pinion and gear, kg (slug)
$N_T$	number of teeth
$P$	tooth load, N (lb)
$p$	pressure in the Hertzian contact, Pa (psi)
$P_d$	dynamic load, N (lb)
$P_F$	load factor = $P_{d, \max} / P_s$
$P_s$	steady tooth load, N (lb)
$R_1, R_2$	pitch radius of pinion and gear, m (in.)
$R_{b1}, R_{b2}$	base radius of pinion and gear, m (in.)
$R_{o1}, R_{o2}$	outside radius of pinion and gear, m (in.)
$T_{B1}, T_{B2}$	bulk surface temperature of pinion and gear, °C (°F)
$T_{F1}, T_{F2}$	total flash temperature, °C (°F)
$T_o$	ambient temperature, °C (°F)
$V$	pitch-line velocity, m/s (in/s)
$X_R$	$\theta_1 R_{B1} - \theta_2 R_{B2}$ , m (in.)
$\alpha$	pressure viscosity coefficient, m <sup>2</sup> /N (in <sup>2</sup> /lb)
$\beta$	temperature viscosity coefficient, K (°R)
$\theta_1, \theta_2$	angular displacement of pinion and gear, rad
$\mu$	lubricant viscosity, cP (lb·s/in <sup>2</sup> )
$\mu_o$	ambient viscosity, cP (lb·s/in <sup>2</sup> )
$\xi_c$	nondimensional damping = $C_o / (2 KM)$
$\varphi$	pressure angle, rad

\*Work performed under NASA Contract NGR 14-007-084.

†International Harvester Co., Hinsdale, Illinois.

‡Northwestern University, Evanston, Illinois.

## Summary of Analyses

The major quantities to be calculated include the dynamic load,  $P_d$ , the minimum film thickness,  $h_{\min}$ , the bulk surface temperature of surfaces 1 and 2 ( $T_{B1}$  and  $T_{B2}$ ), and the total flash temperature in the contact for surfaces 1 and 2 ( $T_{F1}$  and  $T_{F2}$ ). Analysis of each of these variables is summarized in the following sections.

### Dynamic Load

The effects of load sharing between a pair of teeth, nonuniform bending stiffness, and tooth profile error on the variations of tooth load along the contact path are determined by using the dynamic model shown in figure 1. In this figure the bending stiffness is a function of the load position along the tooth profile and is determined by a finite-element code. Figure 2 shows the nondimensional reciprocal of the stiffness for different tooth loading positions is a function of number of teeth. Using the stiffness data, the following second-order differential equation can be solved numerically for the relative displacement along the contact path  $X_R$ .

$$M \frac{d^2 X_R}{dt^2} + C_o \frac{dX_R}{dt} + K_a(X_R - e_a) + K_b(X_R - e_b) = P_s \quad (1)$$

Once  $X_R$  is solved, the dynamic load is simply

$$P_d = K_a(X_R - e_a) + K_b(X_R - e_b) \quad (2)$$

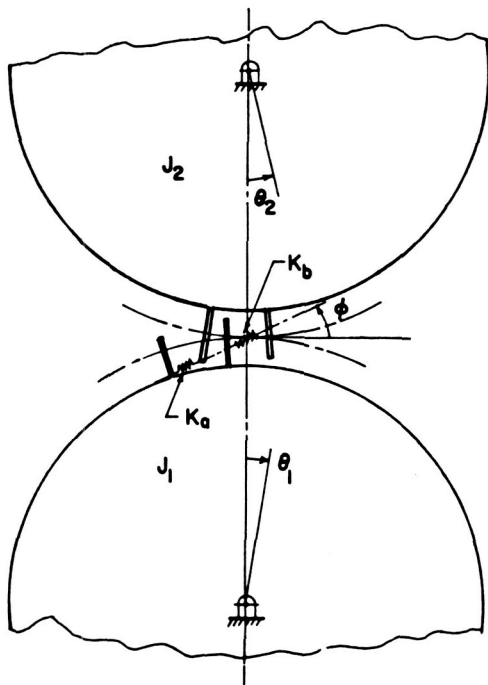


Figure 1. - Dynamic model of meshing gears.

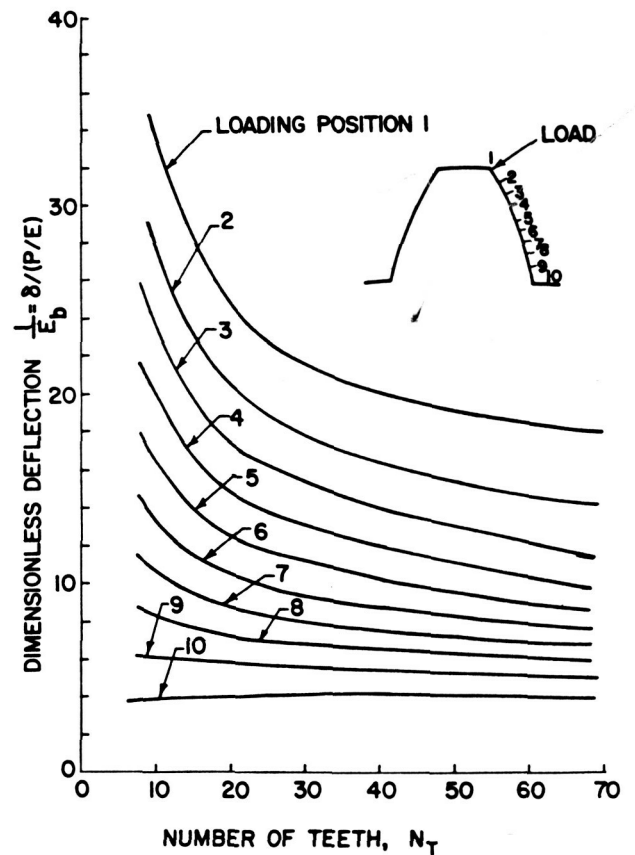


Figure 2. - Dimensionless deflection as function of gear teeth number and loading position.

### **Lubricant Film Thickness**

The calculation of lubricant film thickness is based on a method introduced by Vichard (ref. 3), which includes the squeeze-film effect due to the change in entrainment velocity, local radius, and contact load along the contact path. The Vichard procedure gives rise to a single first-order differential equation in  $h$  with the coordinate along the contact path as the independent coordinate. This was solved by the Runge-Kutta procedure, and the detailed equation and solution procedure can be found in reference 1.

### **Flash Temperature**

At a given contact point along the contact path, the flash temperature distribution on each of the two surfaces within the Hertzian region is solved by considering a heat-conduction analysis of the lubricant film separated by the contacting surfaces. Two major assumptions are used in the analysis. First, the heat generated by shearing of the lubricant is concentrated at the midplane of the lubricant film and is governed by the limiting shear-stress model introduced by Dyson (ref. 4). This leads to a triangular temperature profile with the maximum tip temperature occurring at the midfilm. Second, both surface temperature rises are governed by the Jaeger solution for a high Peclet number (ref. 5). These considerations give rise to three simultaneous equations which can be solved for the two flash surface temperatures and the midfilm shear stress. Details of these three equations are given in reference 1.

### **Bulk Surface Temperature**

The bulk surface temperature is the steady-state temperature distribution along the tooth profile after many cycles of running. The distribution of the bulk temperature can be predicted by a steady-state conduction analysis for a heat flux along the contact side of the tooth facing equivalent to the total heat per mesh averaged over the entire cycle of revolution. Since this temperature computation must be repeated for every iteration, it is more economically handled by using the temperature influence coefficients, which are obtained independently using a finite-element code specially written for the spur gear geometry. The coefficient matrix is determined by solving the temperature profile with a unit heat flux at each point along the tooth profile.

### **Numerical Procedure**

The dynamic load is practically unaffected by the film thickness or the surface temperature; it can be solved independently. The remaining three quantities are coupled and are solved by an iterative process. The overall computational scheme can be best described by a flow diagram shown in figure 3. This is used in constructing a computer program entitled "TELSGE" (Thermal Elastohydrodynamic Lubrication of Spur Gears). The function of each subroutine is described as follows:

(1) The scheme begins with subroutine INPU, which enters all input data including gear geometry, material properties, lubricant properties, and operating conditions such as speed, load, and ambient temperature.

(2) The program then executes subroutines PICK and INVGEN, which are used to obtain the matrix of influence coefficients for calculating the equilibrium surface temperature distribution along the contacting profile. This is achieved by interpolation of a stored data bank of influence coefficients.

(3) After INVGEN the program executes subroutine COGEN, which is used to generate the coordinates of a mesh of quadrilateral elements in a typical gear segment.

(4) Subroutine DYNALO is then executed, and it computes the dynamic load by integrating equation (1).

(5) The program then begins the iterative loop to solve for the flash temperature and the equilibrium surface temperature. Subroutine FILM is first executed, and it calculates the film thickness by integrating the transient film equation.

(6) The flash temperature on each contacting surface and the heat flux distribution are determined in subroutine FLASH by solving a system of three algebraic equations at each grid within the Hertzian contact.

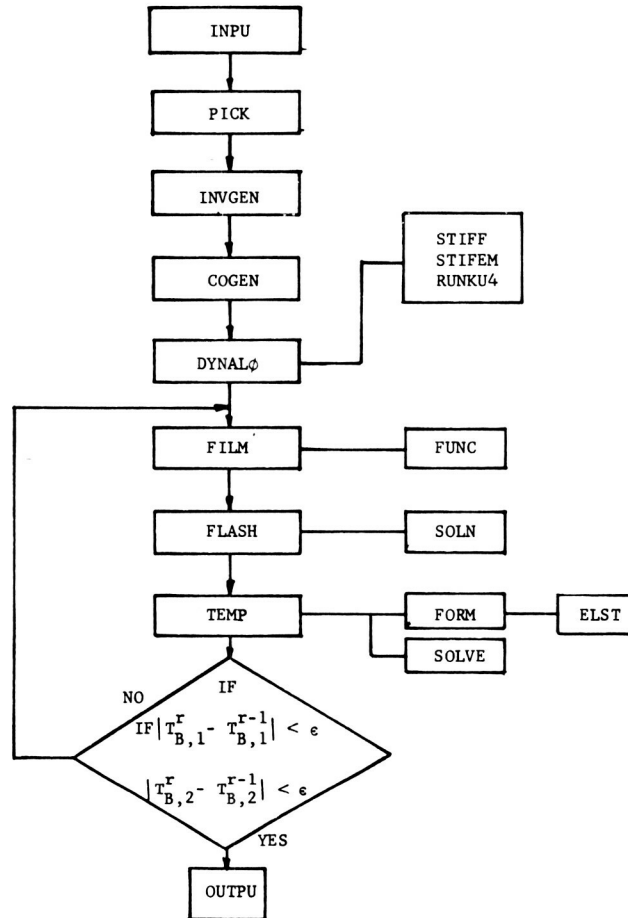


Figure 3. - Flow diagram.

(7) In subroutine TEMP the equilibrium temperature distribution on the contacting surface is computed by using the influence coefficients obtained in subroutine INGEN for the distribution of the heat flux calculated in subroutine FLASH. The newly iterated values of equilibrium temperature are compared with the values in the last iteration. If the difference at every node on the surface is within the allowable error, the iteration is considered to be converged. If not, the procedure is repeated at subroutine FILM.

(8) Subroutine OUTPU prints out all the output data of the dynamic load, film thickness, flash temperature, and the equilibrium surface temperature along the contacting path.

### Dynamic Load Variation

In general, the dynamic load distribution deviates from the static load distribution and is found to change greatly with the operating speed. The relationship of dynamic load variation with speed as well as with gear geometrical factors is described in the following sections.

For gears with true involute profiles under normal operating conditions, the main excitation to the system originates from the periodical change in teeth stiffness due to the alternating engagement of single and double pairs of teeth. The resulting mode of vibration is therefore dependent on the frequency of this forcing excitation and, hence, is dependent on the operating speed. Figure 4 shows dynamic load variation in three speed regions for a pair of 28-tooth and 8-pitch gears.

In the low-speed region, where the excitation frequency from the change of stiffness is much lower than the resonating frequency of the system, the dynamic load response is basically a static load

sharing in phase with the stiffness change, superimposed by an oscillatory load at a frequency corresponding to the system's resonating frequency.

As the speed increases to the neighborhood of the resonance, the typical load response (fig. 4(b)) contains load variations so abrupt that they sometimes can even produce teeth separation. In this speed region the peak dynamic load is much higher than the input static load and is very likely a source of gear noise and early surface fatigue. Operating in this region is obviously harmful. As the speed increases beyond the frequency of the resonating frequency, the dynamic load becomes out of phase with the stiffness variation, and it has a much smoother response. The peak of this load response is much reduced and is smaller than the static load. The shape of this load response (fig. 4(c)) is usually preserved with further speed increases.

### Effect of Speed

One of the approaches to investigate the effects of various parameters on this dynamic load is through the use of dynamic load factor,  $P_F = P_{dmax}/P_s$ , where  $P_s$  is the static load and  $P_{dmax}$  is the maximum dynamic load along the line of action or the contacting path. The effect of speed is exemplified by plotting  $P_F$  against the frequency ratio  $\omega_r = \omega_n$ , defined as the ratio of the excitation frequency,  $\omega$ , due to the periodical change of tooth stiffness to the system's natural frequency,  $\omega_n$ . The system natural frequency  $\omega_n$  is taken as the frequency at which the maximum dynamic load occurs.

Figure 5 shows a typical curve of the dynamic load factor  $P_F$  versus frequency ratio  $\omega_r$ . The general trend of the response is similar to that of a single-degree-of-freedom, forced vibratory system

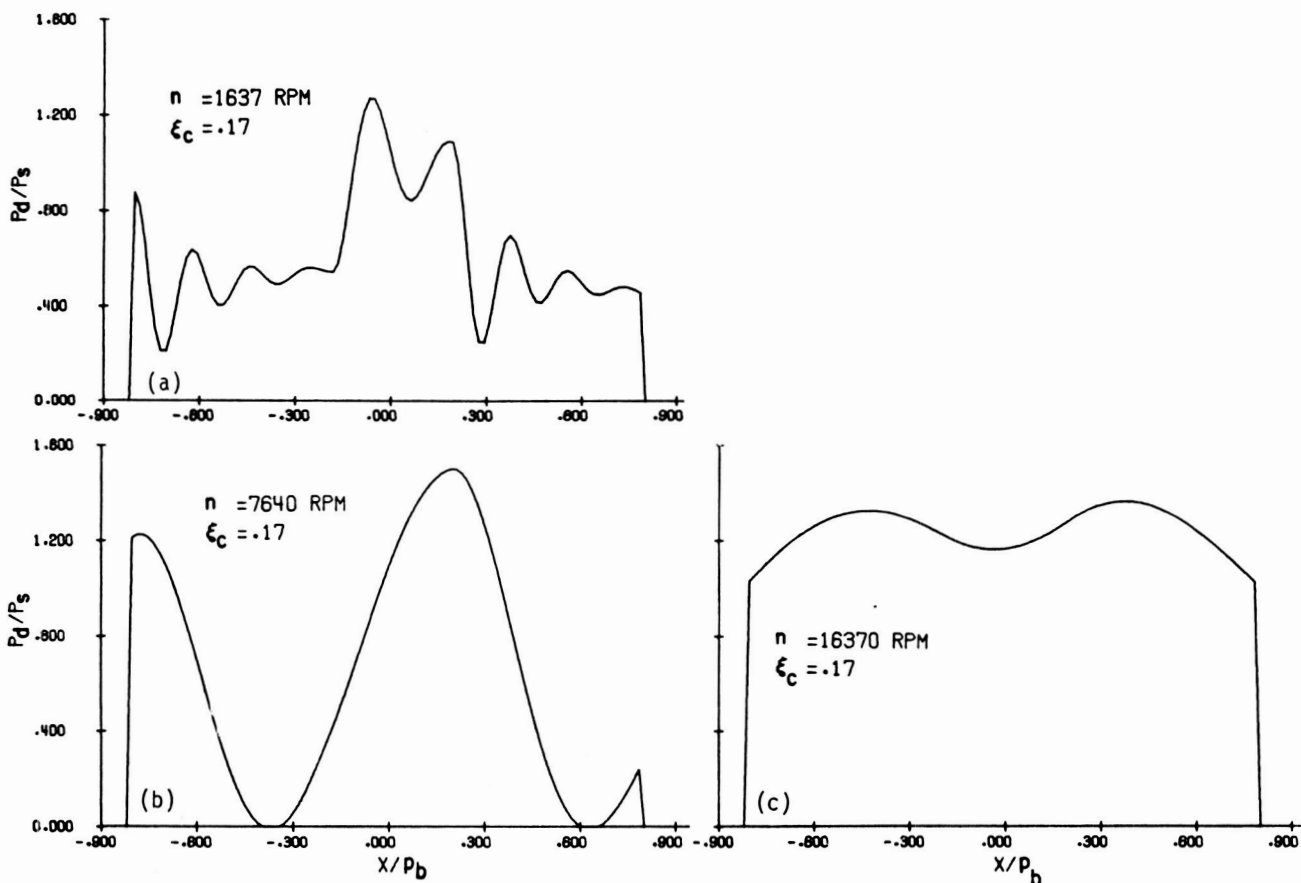


Figure 4. - Dynamic load variation;  $r_G = 1$ ;  $N_T = 28$ ;  $D_p = 8$ ;  $D = 0.254$  cm (0.1 in.). (a)  $n = 1637$  rpm; (b)  $n = 7640$  rpm; (c)  $n = 16370$  rpm.

except that a few secondary peaks of the dynamic load ratio exist in the region of  $\omega_r < 1$ . When  $\omega_r$  approaches unity, the load rises rapidly exhibiting a resonating phenomenon. For speeds above the natural frequency, the dynamic load decreases steadily in the same manner as the ordinary vibratory system.

### Effect of Damping Ratio $\xi$

The damping coefficient  $C_o$  governing the dynamic load variation depends on the viscous friction of the gear system. It is usually an unknown. The damping ratio  $\xi_c$  in the present analysis is defined as  $\xi_c = C_o / 2 \sqrt{KM}$ . An arbitrary value between 0.1 and 0.2 was used in the analysis reported by Hirano (ref. 6) and Ishikawa (ref. 7) for the correlation between their analytical and experimental results. To explore the effect of this ratio, arbitrary values of 0.1, 0.17, and 0.2 were used to generate the dynamic load ratios shown in figure 6. As observed in this figure,  $\xi_c$  has a major influence on  $P_F$  when the operating speed is close to the resonating frequency. Away from the resonance  $\xi_c$  has little influence on  $P_F$ .

### Effect of Contact Ratio

Contact ratio is defined as the ratio of the contact length to the base pitch. This ratio measures the duration of load being shared by more than one pair of teeth, and it has a considerable effect on the dynamic load response. For gears with different diametral pitches, the dynamic load response is different because of the change in contact ratio. It is expected that an increase in contact ratio would have a beneficial effect on the load sharing. To verify this fact, a comparison is made of the dynamic load responses of gears having 8-pitch and 16-pitch under identical operational conditions. The corresponding contact ratios for these two sets of gears are 1.64 and 1.78, respectively. As shown in figure 7, the five pitch gears (16-pitch) having a higher contact ratio have a smaller dynamic load compared with that calculated for coarser gears.

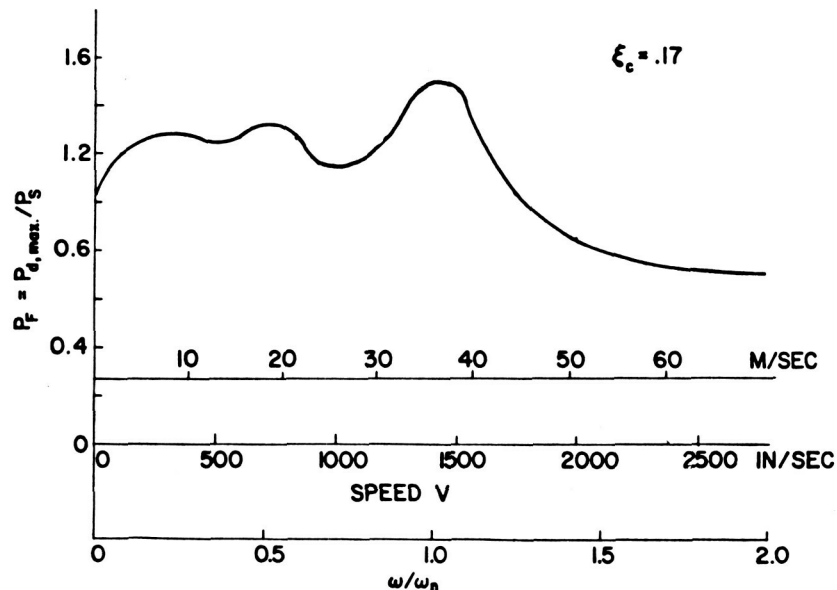


Figure 5. - Effect of speed and dynamic load factor;  $r_G = 1$ ;  $N_T = 28$ ;  $D_p = 8$ ;  $D = 0.254$  cm (0.1 in.).

## Lubrication Performance

The computer code developed is applicable for a wide range of geometric, material, and operating parameters. In this section typical results were generated for a set of gears having a geometry similar to that used by Townsend and Zaretsky (ref. 8). These results cover effects of geometrical factors including face width, gear size, diametral pitch, gear ratio, and tip relief. In addition, the effects of lubricant viscosity, heat-transfer coefficient, speed, and load on the lubrication performance are also included.

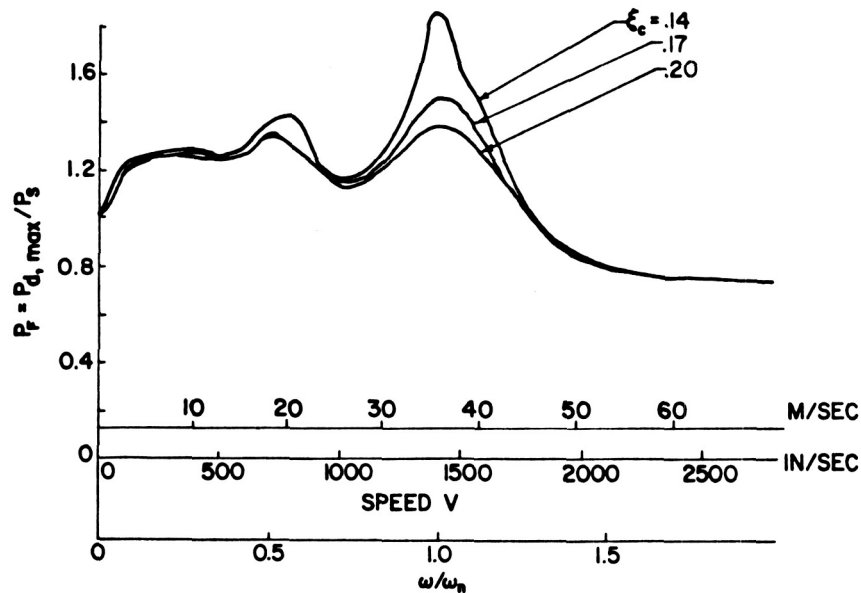


Figure 6. - Effect of damping ratio on dynamic load factor;  $r_G = 1$ ;  $N_T = 28$ ;  $D_p = 8$ ;  $D = 0.254$  cm (0.1 in.).

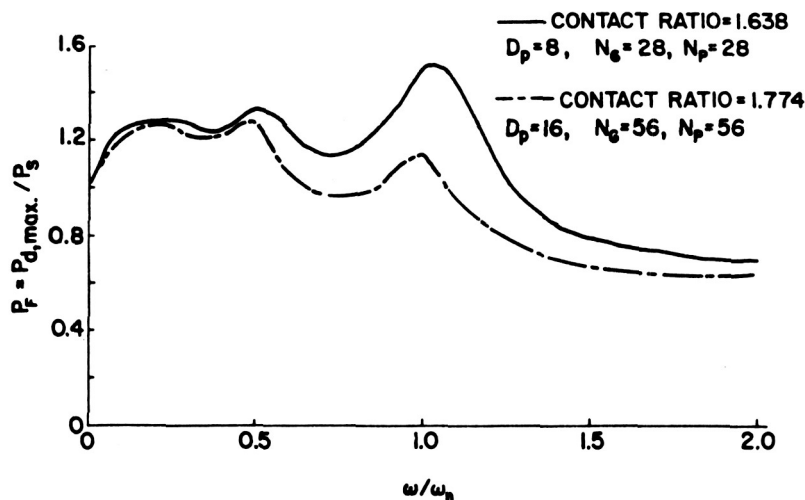


Figure 7. - Effect of contact ratio on dynamic load.

## Distribution of Equilibrium Temperature, Total Flash Temperature, and Minimum Film Thickness

In this section detailed distributions of the minimum film thickness and temperature are plotted against the contact position for a set of gears and the lubricant used in reference 8. The properties of the lubricant as well as the geometry of the gears are listed in table I. In determining the distribution of minimum film thickness, it was assumed that the minimum film in a Hertzian contact is 75 percent of the plateau film thickness calculated from the transient film equation.

The detailed equilibrium surface temperature on both the pinion and gear teeth contacting surfaces is shown in figure 8 in terms of contact position  $X$ , when  $X = X_R/R_i$  and  $R_i$  is the effective radius at the pitch point. It is seen that the equilibrium temperatures for both the pinion and the gear are higher at the tip of the tooth than at the root. This results in a pronounced temperature differential between the tooth surfaces during the beginning and the ending of the engagement.

The total flash temperatures as a function of the contacting position are plotted in figure 9 for three speeds. At speeds below or near the resonance, the total flash temperature shows local fluctuations of total flash temperature are not found at a speed considerably above the resonance.

The corresponding dynamic film thickness for this case is shown in figure 10 as a function of tooth contact position. The squeeze film effect is shown to be only important at a very short period after the teeth are engaged. Examinations of the film thickness distributions for all other runs indicate that the squeeze film effect is indeed not a dominant effect on the minimum film thickness.

### Effect of Gear Geometry

The results in the previous section show the detailed distributions along the contact path. In the following sections one is concerned with the overall performance as affected by the change of geometrical factors. The overall performance is represented by three quantities, the maximum equilibrium surface temperature  $T_{B,max}$ , the maximum total flash temperature  $T_{F,max}$ , and the minimum film thickness  $h_{min}$  along the contacting path.

Investigating the effects of gear geometry, the first case considered is the effect of gear face width. Borsoff (ref. 9) found experimentally that the increase of face width would reduce the specific load carrying capacity (load per unit face width). This phenomenon does not seem to be explainable

TABLE I. – GEAR DATA, LUBRICANT DATA, AND STANDARD OPERATING CONDITIONS

#### (a) Gear data

Number of teeth, $N_T$ .....	28
Diametral pitch, $D_p$ .....	8
Pressure angle, $\phi$ , deg.....	20
Pitch radius, $R_1$ , cm (in.).....	4.445 (1.75)
Outside radius, $R_{o1}$ , cm (in.).....	4.7625 (1.875)

#### (b) Lubricant (Superrefined naphthenic mineral oil) data

Kinematic viscosity, $\text{cm}^2/\text{sec}$ (cs), at—	
311 K (100° F).....	0.73 (73)
372 K (210° F).....	0.077 (7.7)
Density at 289 K (60° F) $\text{g}/\text{cm}^3$ .....	0.8899
Thermal conductivity at 311 K (100° F), $\text{J}/(\text{m})(\text{sec})(\text{K})$ (Btu/(hr)(ft)(°F)).....	0.0125 (0.0725)
Specific heat at 311 K (100° F), $\text{J}/(\text{kg})(\text{K})$ (Btu/(lb)(F)).....	582 (0.450)
Lubricant viscosity at temperature equation.....	$\mu = \mu_o \exp[\alpha p + \beta(1/T - 1/T_o)]$
Pressure viscosity coefficient, $\alpha$ , $\text{m}^2/\text{N}$ (in <sup>2</sup> /lb).....	$2.3 \times 10^{-7}$ (0.00016)
Temperature viscosity coefficient, $\beta$ , K (°R).....	3890 (7000)

#### (c) Standard operating conditions

Load per unit width, $P$ , N/m (lb/in).....	0.753 (4300)
Pitch line velocity, $V$ , m/sec (in/sec).....	46.55 (1832)
Ambient temperature, $T_o$ , °C (°F).....	37.78 (100)
Surface heat transfer coefficient, $\text{W}/\text{m}^2\text{K}$ (Btu/(ft <sup>2</sup> )(hr)(R)).....	341 (60)

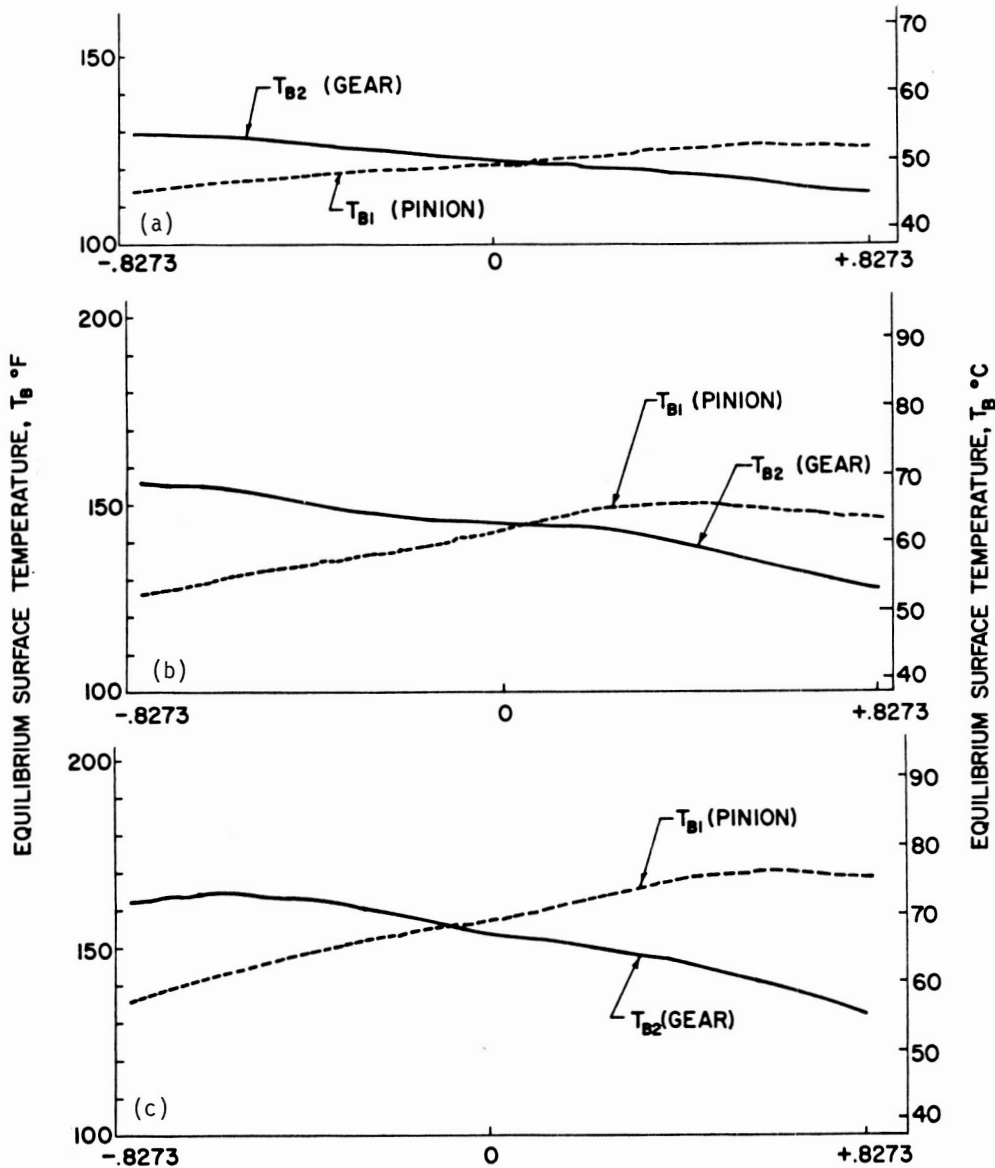


Figure 8. - Distribution of equilibrium surface temperature;  $r_G = 1$ . (Other conditions are listed in table I.) (a)  $n = 1637$  rpm; (b)  $n = 7640$  rpm; (c)  $n = 16370$  rpm.

by Blok's flash temperature theory or by any existing EHD film thickness theory. As shown in figure 11, the present results indicate that, as the face width increases from 0.05 to 0.2 in., under the same load there is a corresponding increase in the maximum equilibrium surface temperature as well as in the total flash temperature. The higher surface temperature results in a much reduced minimum film thickness when the face width is increased. This suggests that the experimental trend obtained by Borsoff with regard to the effect of face width can be at least partially accounted for by the present analysis on the basis of its effect on the surface temperature and film thickness.

The effect of gear outside radius is shown in figure 12. It is seen that when the pitch-radius is increased from 1.75 to 2.5 in., under a constant load and speed, the total flash temperature as well as the film thickness is considerably improved. However, one must keep in mind that the improvement in lubrication performance by increasing the size of gears is a rather expensive way to solve the lubrication problem.

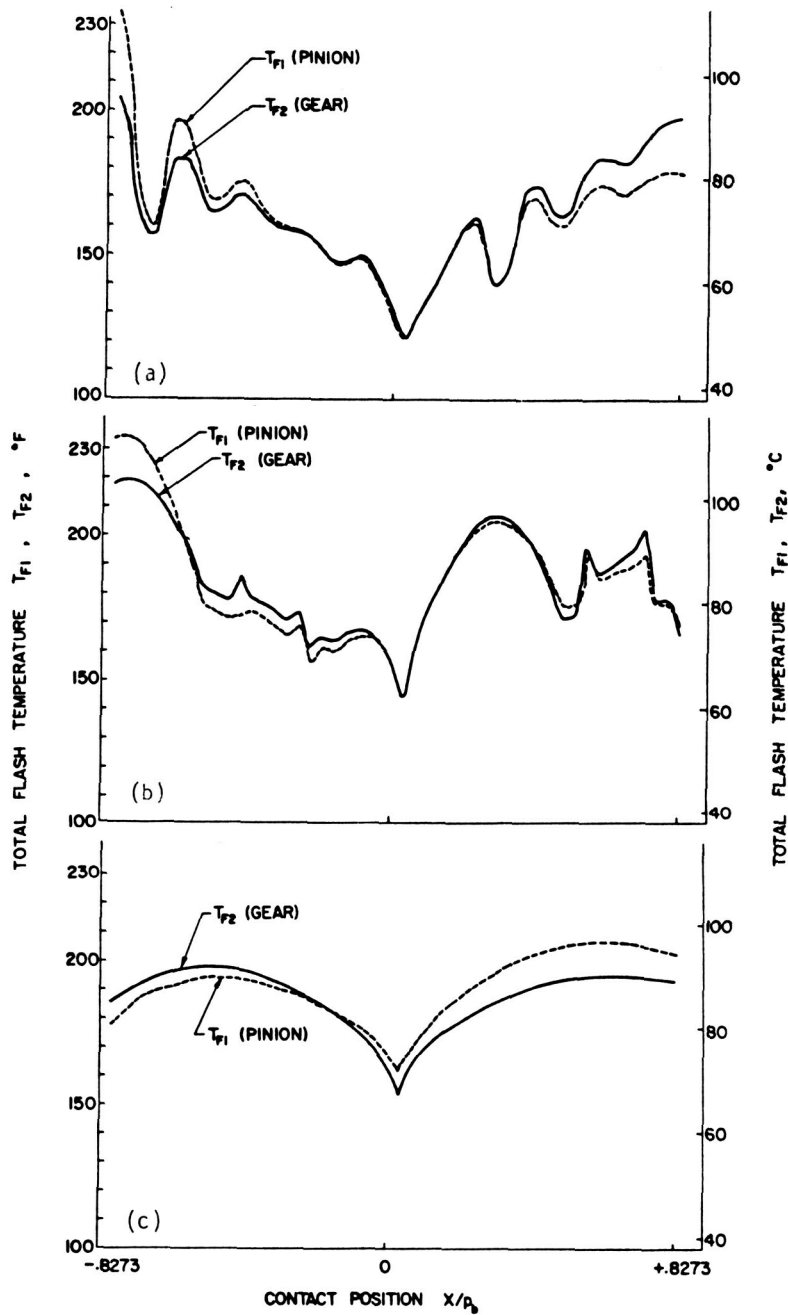


Figure 9. - Distribution of total flash temperature;  $r_G = 1$ . (Other conditions are listed in table I.) (a)  $n = 1637$  rpm; (b)  $n = 7640$  rpm; (c)  $n = 16370$  rpm.

The effect of diametral pitch is shown in figure 13. Since an increase in diametral pitch tends to reduce the dynamic load and the sliding between teeth, the use of gears with a finer pitch yields a lower maximum surface temperature as well as a lower total flash temperature, in comparison with the corresponding values for coarser gears. The minimum film thickness is also found to be much improved as the diametral pitch changes from 8 to 12. However, it must be kept in mind that the improvement in lubrication performance in this instance can be easily offset by the reduction in flexural strength for gears with a finer pitch.

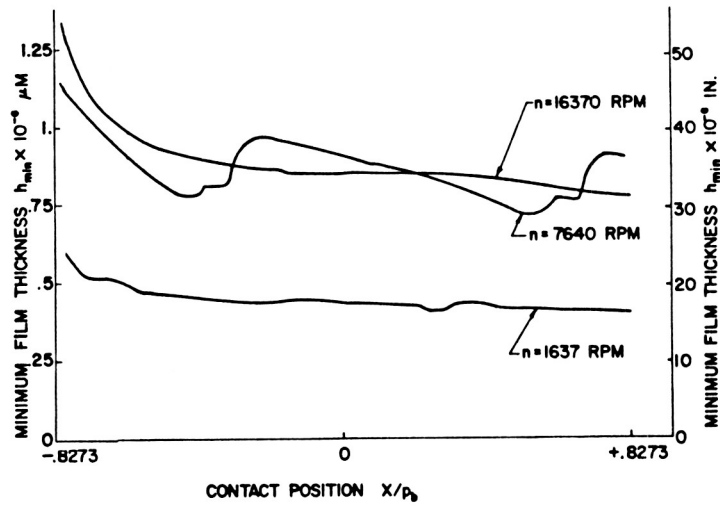


Figure 10. - Dynamic film thickness distribution.

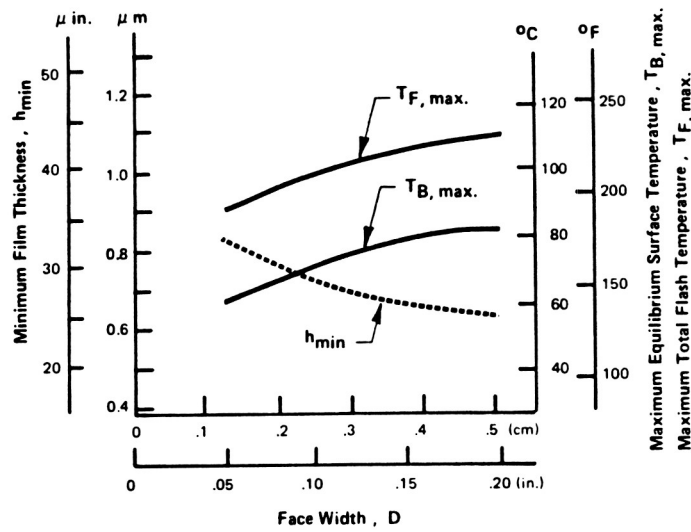


Figure 11. - Effect of face width on lubrication performance.

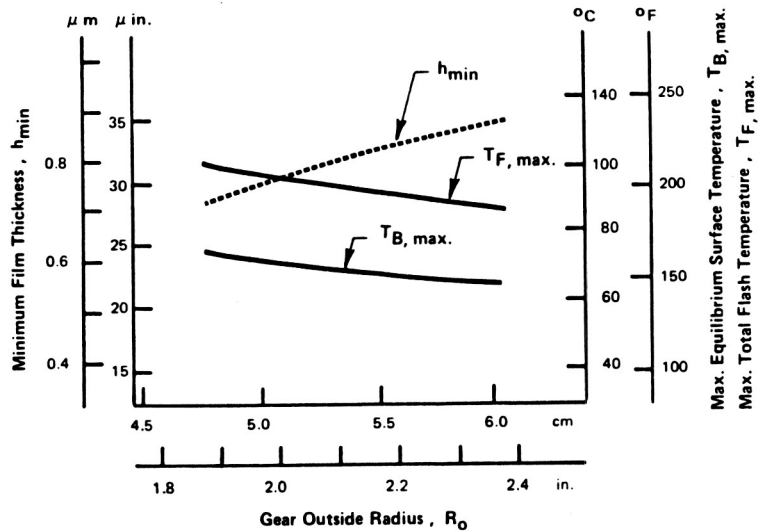


Figure 12. - Effect of gear outside diameter on lubrication performance.

Figure 14 shows the effect of gear ratio on the lubrication performance. The gear ratio is varied from 1 to 2 by increasing the gear teeth number from 28 to 56. It is seen that the increase in the size tends to improve the cooling effect and hence reduce both the equilibrium temperature and the total flash temperature. The effect on film thickness is even greater because of a larger effective radius in the Hertzian contact.

### Effect of Lubricant Operating Parameters

Aside from the effects of gear geometry, lubricant properties and the gear operating conditions are also known to have an influence on the gear lubrication performance. The effect of lubricant viscosity is shown in figure 15. When the lubricant viscosity is increased from 0.062 to 0.1379 Pa·s ( $9 \times 10^{-6}$  to  $20 \times 10^{-6}$  lb·sec/in<sup>2</sup>), the film thickness is found to have a marked increase, and it is accompanied by a slight increase in maximum equilibrium and total flash temperature on the surface. This indicates that the reduction in load carrying capacity in practice for gears with low viscosity oils is likely caused by the lack of lubricant film in the contact.

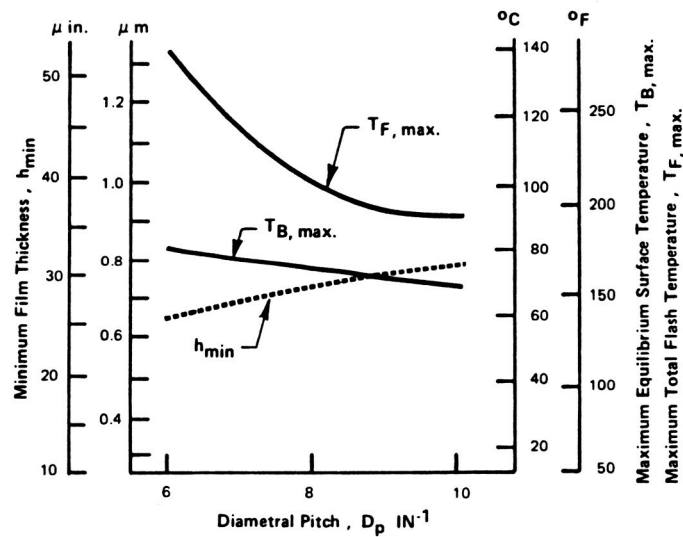


Figure 13. - Effect of diametral pitch on lubrication performance.

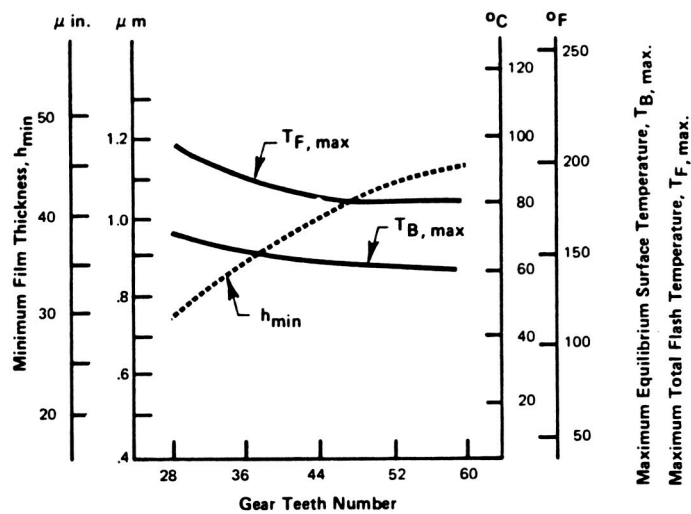


Figure 14. - Effect of gear ratio on lubrication performance pinion teeth. Number = 28.

The effect of surface convective heat-transfer coefficient and the effect of ambient temperature on the lubricant performance are shown separately in figures 16 and 17. Increasing the heat-transfer coefficient or decreasing the operating ambient temperature is shown to have a substantial improvement on the lubrication performance.

Among the effects of operating parameters, perhaps the most interesting one is the speed effect. Figure 18 shows the results on the effect of speed for the same set of gears considered in the preceding sections. It is seen that as the pitch-line speed increases from 21.1 to 72.0 m/sec (830 to 2832 in/sec) the minimum film thickness experiences a gradual increase, which appears to be sustained throughout the high-speed region. The corresponding total flash temperature also shows a slight improvement with speed in spite of a gradual increase in the equilibrium temperature. This trend seems to be in accord with the experimental evidence provided by Borsoff (ref. 9) and Ku and Baber (ref. 10) in which they concurred that the scuffing load capacity increases gradually with speed in the high-speed region.

The results by varying the tooth load from 0.753 to 1.103 MN/m (4300 to 6300 lb/in) are plotted in figure 19. It is seen that the minimum film decreases linearly with the load but that the equilibrium temperature as well as the total flash temperature increases also linearly with the load.

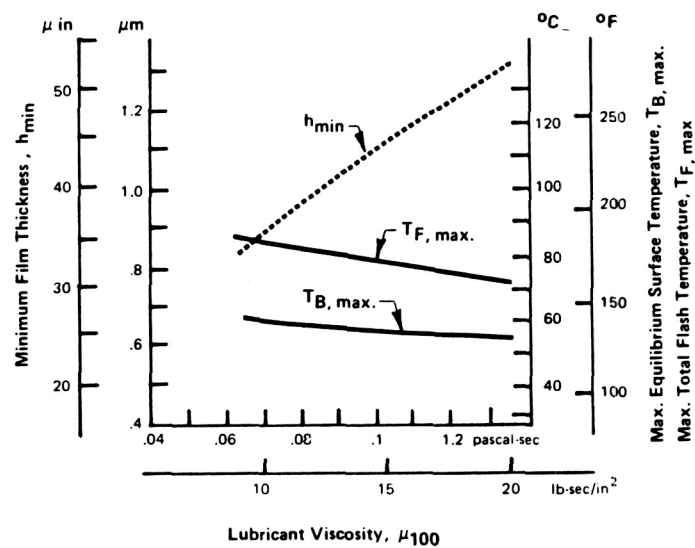


Figure 15. - Effect of lubricant viscosity on lubrication performance;  $P = 0.7$  MN/m (400 lb/in),  $D = 0.127$  cm (0.05 in.).

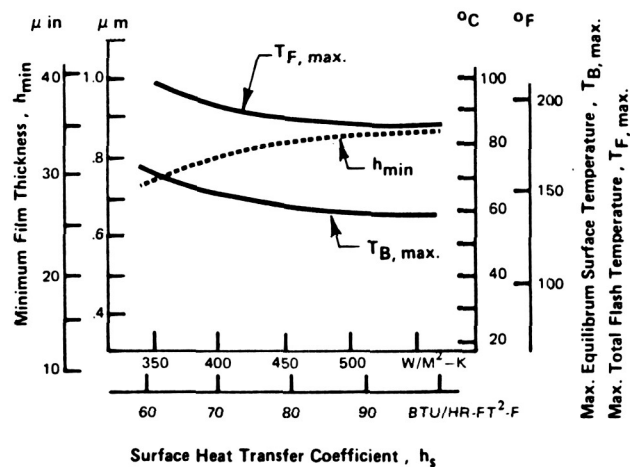


Figure 16. - Effect of surface heat transfer coefficient on lubrication performance.

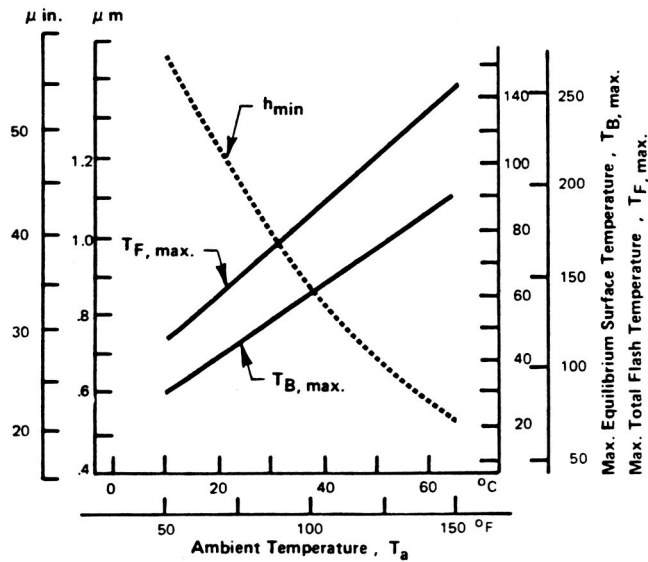


Figure 17. - Effect of ambient temperature on lubrication performance.

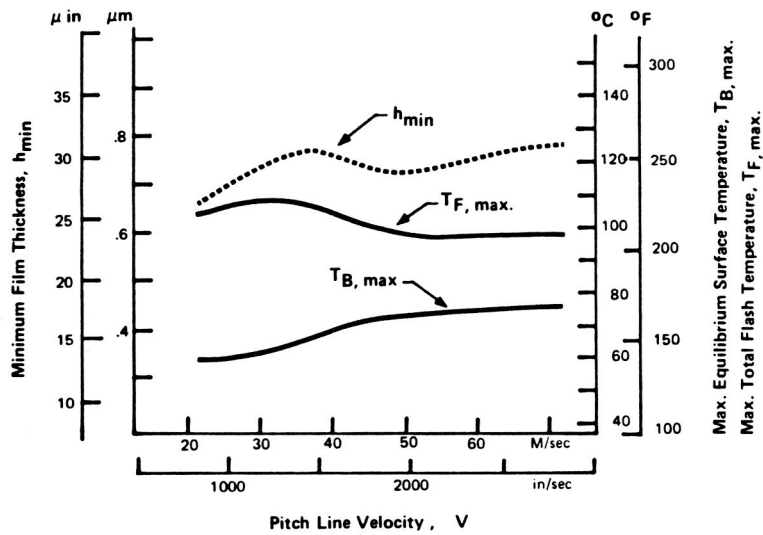


Figure 18. - Effect of surface speed on lubrication performance.

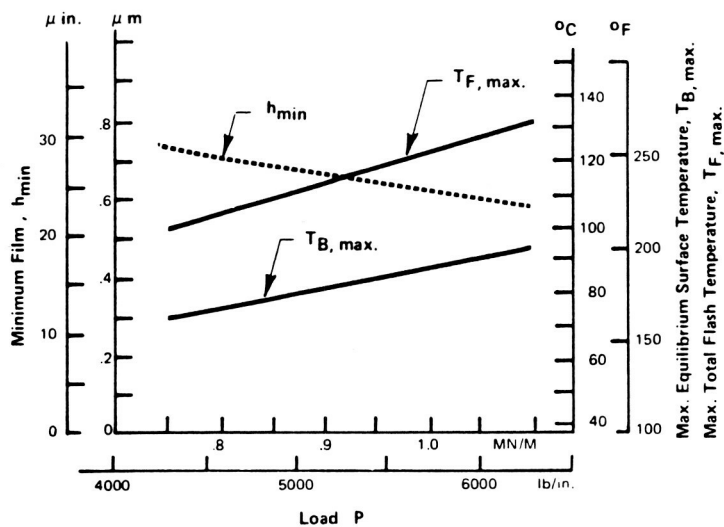


Figure 19. - Effect of load on lubrication performance.

## Summary of Results

Results of dynamic load were obtained for a pair of gears with dimensions corresponding to that used by Townsend and Zaretsky (ref. 8) in their gear experiments. The dynamic load distributions along the contacting path for various speeds show patterns similar to that observed experimentally. Effects of damping ratio, contact ratio, on the dynamic load were examined.

Gear lubrication performance was evaluated by plotting the maximum bulk equilibrium temperature, the maximum total flash temperature, and the minimum film thickness along the contacting path for various geometric and operating parameters. It was found that an increase in diametral pitch or a decrease in face width for the same specific load gives a better lubrication performance. These trends agree qualitatively with experimental results by Borsoff (ref. 9) and by Ku and Barber (ref. 10). Among the operating variables, the lubrication performance is improved most strongly by increasing the inlet lubricant viscosity, by decreasing the ambient temperature, or by increasing the convective heat-transfer coefficient on the gear surface. Increasing the pitch-line velocity gives a slight improvement in lubrication performance at high speeds. However, the trends do not indicate any signs which can account for the dramatic increase in scuffing load observed by Borsoff at very high speeds.

## References

1. Wang, K. L.; and Cheng, H. S.: A Numerical Solution to the Dynamic Load, Film Thickness, and Surface Temperatures in Spur Gears, Part I—Analysis. *J. Mech. Des.*, vol. 103, Jan. 1981, pp. 177-87.
2. Wang, K. L. and Cheng, H. S.: A Numerical Solution to the Dynamic Load, Film Thickness, and Surface Temperatures in Spur Gears, Part II—Results. *J. Mech. Des.*, vol. 103, Jan. 1981, pp. 188-94.
3. Vichard, J. P.: Transient Effects in the Lubrication of Hertzian Contacts. *J. Mech. Eng. Sci.*, vol. 13, no. 3, 1971.
4. Dyson, A.: Frictional Traction and Lubricant Rheology in Elastohydrodynamic Lubrication. *Philos. Trans. Royal Soc. (London)*, Ser. A, vol. 266, 1970, pp. 1-33.
5. Jaeger, J. C.: Moving Sources of Heat and Temperature at Sliding Contacts. *J. Proc. Roy. Soc. N.S.W.*, vol. 76, 1942, pp. 203-224.
6. Ichimaru, K.; and Hirano, I.: Dynamic Behavior of Heavy-Loaded Spur Gears. ASME Paper No. 72-PTG-14, 1972.
7. Ishikawa, J.; Hayashi, K.; and Yokoyana, M.: Surface Temperature and Scoring Resistance of Heavy-Duty Gears. ASME Paper No. 72-PTG-22, 1972.
8. Townsend, D. P.; and Zaretsky, E. V.: A Life Study of AISI M-50 and Super Nitralloy Spur Gears With and Without Tip Relief. ASME Paper No. 73-Lub-30, 1973.
9. Borsoff, V. N.: On the Mechanism of Gear Lubrication. *J. Basic Eng.*, vol. 80D, 1959, pp. 79-93.
10. Ku, P. M.; and Barber, B. B.: The Effect of Lubricants on Gear Tooth Scuffing. *ASLE Trans.*, vol. 2, no. 2, Oct. 1959.